Proceedings of 14th IOE Graduate Conference
Peer Reviewed
Year: 2023 Month: December Volume: 14
ISSN: 2350-8914 (Online), 2350-8906 (Print)

Design and Setup of Z-type Schlieren Imaging System for Flow Visualization

Salim Maharjan [a], Kamal Darlami [b], Laxman Poudel [c]

[a, b, c] *Department of Mechanical and Aerospace Engineering, Pulchowk Campus, IOE, Tribhuvan University, Nepal*

[a] 078msmde013.salim@pcampus.edu.np, [b] darlami.kd@pcampus.edu.np, [c] laxman@ioe.edu.np

Abstract

Amid the research works in the field of aerodynamics and flow physics, visual experiments become a key aspect to understand the physics behind the phenomenon at work. Owing to the sensitivity of phenomenon involved in those fields, non-intrusive techniques hold greater preference over intrusive techniques. Schlieren photography is one example of non-intrusive technique, used for the qualitative and quantitative analysis of different fluid-flow phenomena involving density gradients. In this study, a portable experimental setup of the z-type schlieren technique sitting in a bench-top of size 90 cm × 90 cm, consisting of two reflecting telescope parabolic mirrors of 7.6 cm diameter and 40 cm focal length is fabricated. With this setup, the qualitative analysis of different flow phenomena were performed. Thermal plumes from a burning candle, flow of heated air near the periphery of a soldering iron rod, and under-expanded jet from a Converging-Diverging (CD) nozzle are used as subjects of investigation. The visualized phenomena range from subsonic characteristic to supersonic characteristic.The setup was able to capture the thermal plume of a burning candle and flow of heated air near the periphery of soldering iron rod with great clarity. In the study of under-expanded jet through a CD-nozzle, the formation of shock diamond structures were observed, meaning the setup is sensitive enough to capture phenomena related to high-speed flow physics as well.

Keywords

Aerodynamics, Flow visualization, Schlieren photography, Shock diamond, Under-expanded jet, Z-type 2-mirror schlieren system

1. Introduction

1.1 Background

The innate inquisitive nature of humans has long pondered over the nature of fluid flows. The experimental and theoretical works carried out by the generation of different scientists in the quest for understanding the panoply of fluid-flow phenomena laid the early foundation of fluid-dynamic research. In many of these researches, visualization of the flow that are being studied is crucial. This is because fluids, gaseous or liquids, are transparent media, and their motion remains invisible to the human eye under direct observation. The techniques allowing for the visualization of fluid-flow is referred to as flow visualization. The methods of flow visualization is classified according to three principles: light scattering from tracer particles, optical methods relying on refractive index changes in the fluid, and interaction processes of the fluid flow with a solid surface [1]. The optical methods which is the main focus of this research are independent of the use of particles/ tracers to visualize the fluid-flow. The examples of optical flow visualization techniques include Schlieren Photography, Shadowgraphy, Moiré Deflectometry, Speckle Photography, Interferometry, etc. Amidst the computational development for fluid dynamics research, there were predictions about optical flow visualization techniques being obsolete by the year 2000. Today the year 2024 is upon us and the computational development in fluid dynamic studies has taken an exponential rise. Amidst all this development, the computational advent has not removed the experimental optical flow visualization methods and those accompanying predictions have been long forgotten. In today's computational dominant era, the ever increasing new computational and numerical methods of solving the fluid-flow problems require a validation counterpart which is generally done by the experimental visualization technique like the optical flow visualization [2]. In retrospect, there has been a symbiotic relation between the improvement of optical flow visualization methods and development in the field of aerospace vehicles and high-speed physics.

Schlieren technique is one of the examples of experimental optical flow visualization technique. It was first brought into public attention by Robert Hooke during the later half of the 17th century. Hooke used a simple system consisting of only one lens and the iris of the spectator's eye as filter as shown in Figure 1. This system was developed to observe the flows of hot air in candle plumes which Hooke demonstrated to the Royal Society of London in 1672. Unfortunately, this method

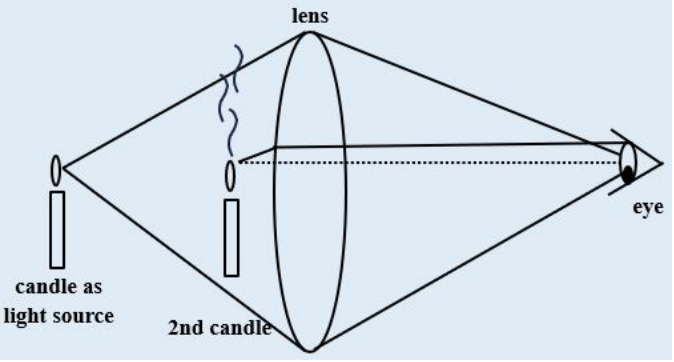

Figure 1: Hooke's schlieren setup

lacked clarity for detailed scientific experimentation and was not revisited for almost 200 years.

Schlieren technique was reinvented and named by August Toepler,1865 and by Leon Foucault at around the same time. Toepler saw schlieren as a scientific instrument that could be used to investigate different fluid-flow phenomena, because it rendered the invisible visible. The schematic diagram of the schlieren setup Toepler developed is shown in Figure 2. He used this technique to look at glasses. The window glasses and optical glasses, viewed with schlieren setup revealed multiple streaks and striations, in German called schliere, and that is how the technique got its name.

The development of the schlieren technique during the 20th century revolves mostly around Hubert Schardin. In his 1934 Ph.D. thesis paper [3], Schardin provided the theoretical framework for the underlying physics of schlieren which was the first of its kind. In the later part of the 20th century, many improvements were introduced in schlieren methods by various scientists and engineers. Amid the new developments color schlieren and monochromatic schlieren methods remain an important optical visualization technique in glimpsing the intricacies of different fluid-flow phenomena, especially those involving density gradients.

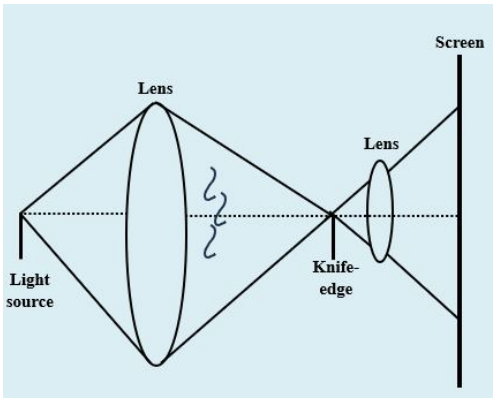

Figure 2: Toepler's single-field-lens schlieren arrangement

(a) **(b)**

Figure 3: (a) Schlieren photograph taken by Ernst Mach and Peter Salcher, (b) Original negative plate with 5-mm-diameter image [4]

Schlieren method has provided the critical visualization in learning important phenomena in the field of physics and engineering. One of such phenomena is the shock wave. Figure 3, taken by Ernst Mach and his colleague Peter Salcher using a schlieren setup, is one of the most famous photographs in the history of experimental physics. It captures the bow shock, tail shock, and turbulent wake of the bullet. This photograph highlighted the hidden intricacies of the supersonic flow thus goose stepping the fluid dynamic research into a new regime where speed was omnipotent.

1.2 Mathematical basis of schlieren theory

The mathematical basis of the schlieren imaging is built following Fermat's principle, also called the principle of least time which states, "light travels between two points along the path that requires the least time". If one considers a ray of light passing through a schlieren object, i.e., a region of inhomogeneities in density/refractive index, Fermat's principle naturally reduces to Snell's law (law of refraction). The light during its propagation upon interacting with a region of variable density gets bent. The refractive index $n = \frac{c_0}{c}$ of a transparent medium indicates this change, where c is the light speed in the medium and c_0 is the light speed in vacuum, 3×10^8 m/s. In the case of air and other gases there is a simple relationship between the refractive index (n) and gas density (ρ):

$$n - 1 = k\rho \tag{1}$$

where k is the Gladstone-Dale coefficient which has a specific value for each gas, and depends weakly on the wavelength of the light used. The mathematical interpretation of schlieren theory could be developed following Figure 4. An illumination which is parallel to the 2D-schlieren object is assumed in x-and y-direction. It is also assumed that there is a negative vertical gradient of refractive index $\partial n/\partial y < 0$, while x- and z-direction does not encounter such gradient. If there is no disturbance, light ray (an electromagnetic wave) propagates in such a way that the wavefront maintains a perpendicular direction to the direction of propagation.Thus, the planar wavefront would be initially vertical upon passing through z_1, and perpendicular to the horizontal optical centerline z. Once the perpendicular wavefront traverses through the schlieren object from z_1 to z_2, it would have covered a differential distance Δz in the differential time Δt. During covering that differential distance, the wavefront would have encountered a deflection of $\Delta\epsilon$. By definition $n = \frac{c_0}{c}$, so the local value of the speed of light c is $\frac{c_0}{n}$, where c_0 is the speed of light in vacuum. From Figure 4, for the small value of ϵ:

$$\tan\Delta\epsilon \approx \Delta\epsilon = \frac{(\frac{c_0}{n_2} - \frac{c_0}{n_1}).\Delta t}{\Delta y} \tag{2}$$

The differential time Δt can be further expressed as:

$$\Delta t = \Delta z.\frac{n}{c_0} \tag{3}$$

Combining Equation 2 and 3,

$$\Delta\epsilon \approx \frac{c_0}{\Delta y}.\left(\frac{n_1 - n_2}{n_1 n_2}\right).\Delta z.\frac{n}{c_0} \tag{4}$$

$$\Delta\epsilon \approx \frac{n}{n_1 n_2}.\left(\frac{n_1 - n_2}{\Delta y}\right).\Delta z \tag{5}$$

$$\frac{\Delta\epsilon}{\Delta z} = \frac{n}{n_1 n_2}.\left(\frac{n_1 - n_2}{\Delta y}\right) \tag{6}$$

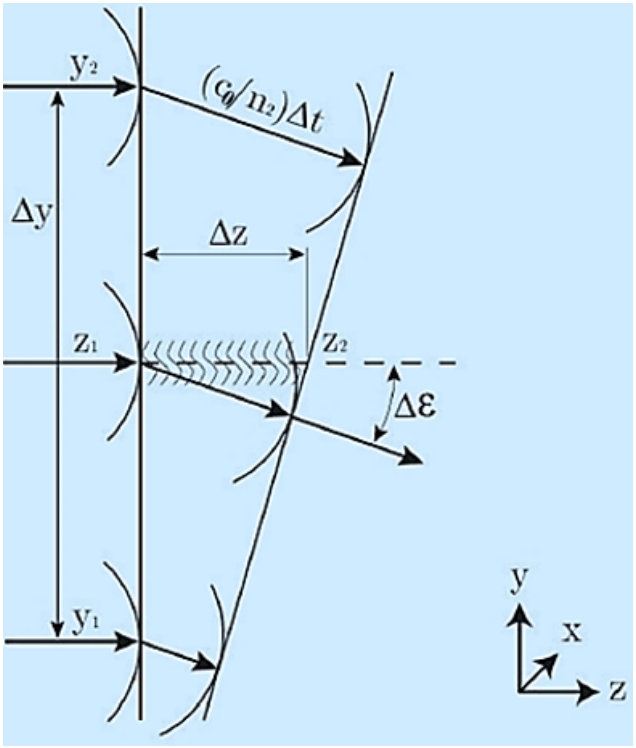

Figure 4: Deflection encountered by a perpendicular light wavefront due to gradient in refractive index $\delta n/dy$

Letting all the finite difference approach zero,

$$\lim_{\Delta z \to 0} \frac{\Delta \epsilon}{\Delta z} \approx \left(\frac{n}{n_1 n_2}\right) . \left(\lim_{\Delta y \to 0} \frac{n_1 - n_2}{\Delta y}\right) \tag{7}$$

$$\frac{d\epsilon}{dz} = \left(\frac{n}{n^2}\right) . \frac{dn}{dy} \tag{8}$$

$$\frac{d\epsilon}{dz} = \frac{1}{n} . \frac{dn}{dy} \tag{9}$$

For small angle approximation:

$$d\epsilon \approx \frac{dy}{dz} \tag{10}$$

Implementing Equation 10 into Equation 9 and writing the total derivatives as partials, one obtains:

$$\frac{\partial^2 y}{\partial z^2} = \frac{1}{n} . \frac{\partial n}{\partial y} \tag{11}$$

Similarly, if there were gradients along the x-direction

$$\frac{\partial^2 x}{\partial z^2} = \frac{1}{n} . \frac{\partial n}{\partial x} \tag{12}$$

Equations 11 and 12 relates the curvature of the refracted ray to the magnitude of the respective refractive-index gradient. Integrating once, the components of the angular ray-deflection in the x- and y-directions are obtained:

$$\epsilon_x = \frac{1}{n} \int \frac{\partial n}{\partial x} \partial z \tag{13}$$

$$\epsilon_y = \frac{1}{n} \int \frac{\partial n}{\partial y} \partial z \tag{14}$$

For two-dimensional schlieren of extent L along the optical axis:

$$\epsilon_x = \frac{L}{n_0} . \frac{\partial n}{\partial x} \tag{15}$$

$$\epsilon_y = \frac{L}{n_0} . \frac{\partial n}{\partial y} \tag{16}$$

where n_0 is the refractive index of the surrounding medium. Equations 11-16 provide the mathematical basis for the schlieren system. Equations 11 and 12 indicate that it is not the refractive index n causing ray deflection, but the gradient $\frac{\partial n}{\partial x}$ or $\frac{\partial n}{\partial y}$ of the refractive index. Additionally, Equations 15 and 16 show that light ray deflections bend towards the region of higher refractive index.

2. Experimental setup of the Z-type 2-Mirror Schlieren System

The experimental setup of the z-type 2-mirror schlieren system is carried out following the fundamental aspects of optics and the physics of refraction. Understanding the basics of the Fourier Optics is particularly helpful in setting up the schlieren system. The Computer-Aided Design (CAD) of the setup in conjunction with the Fourier Optics is shown in Figure 5 and 6.

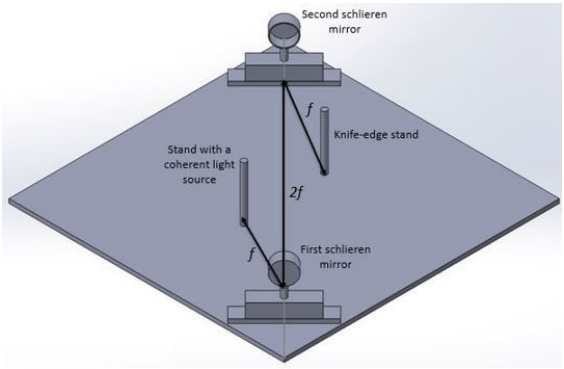

Figure 5: CAD model of the z-type schlieren setup

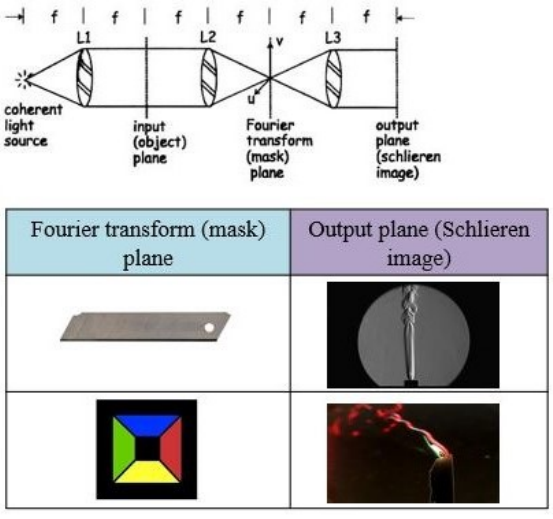

Figure 6: Working of a Fourier Optical Processor

The Fourier Optical Processor starts off with a coherent point light source which is directed towards the first lens kept at one focal length (f) distance away from the point light source. The first lens then produces a collimated beam which refers to a planar wavefront which is brought to a focus by the second lens kept at $2f$ distance away from the first lens. The space in between the two lenses is the test-region where certain disturbances are introduced. That disturbance in schlieren imaging could be thermal plume of a burning candle, under-expanded flow through a nozzle or some heat-transfer phenomena. The light brought to the focus by the second lens produces what is called the Fourier Spatial Frequency Spectrum. If a certain flow-phenomena initiating density-gradient is introduced in the test-region, one would obtain a spectrum of lower and higher frequencies and what the schlieren technique does is to basically truncate that part of the spectrum. Usually, half of the Fourier Spatial Frequency Spectrum is blocked off resulting in a sensitive schlieren image in the output plane. In practice, a razor-blade or a color filter works just fine. In the z-type schlieren system, the lenses are replaced with mirrors and the orientation mimics a z-shape instead of a linear-pattern. In addition to this, certain angle is maintained between the light source and the first schlieren mirror, and between the second schlieren mirror and the knife edge. The other parameters are maintained the same as in Fourier Optical Processor.

2.1 Numerical Calculation

2.1.1 Distance between the mirrors

The mirror chosen for the schlieren setup is a reflecting telescope primary mirror with diameter of 7.6 cm and focal length of 40 cm. The minimum distance between the two mirrors should be $2f$ [5], i.e., 80 cm. Since longer distances do not matter in principle, a distance of 100 cm is kept for providing adequate space for the test-region.

2.1.2 Mirror tilt angle

Based on the assumption that the foci of the schlieren mirrors coincide with the extreme edge of the parallel beam impinging upon it as shown in Figure 7, the angle between the incoming and outgoing beam is given by:

$$\tan(2\theta) = \frac{d}{2f} \tag{17}$$

where d is the diameter of the mirror and f is the focal-length of the mirror. Substituting the values of diameter (d) and focal length (f) of the mirror in Equation 17, the angle between the incoming and outgoing beam is obtained to be 5.42°. This is an impractical situation though. As stated in [5], one needs to have enough test area to work with while maintaining the beam angles small. The value was increased to 15°allowing for a better working space without the interference of the point source in the test area. Since the mirror tilt angle is half of the angle between the incoming and outing beam [5], this yields the mirror tilt angle of 7.5°.

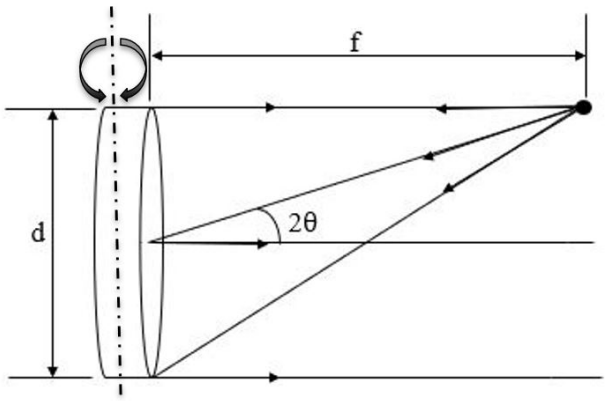

Figure 7: Condition where the foci of the mirrors just coincide with the edges of the parallel beam

2.1.3 Astigmatism severity

In z-type schlieren system the symmetry of on-axis mirrors is thwarted, and this results in aberration called astigmatism. The word astigmatism is a combination of Greek words meaning 'without' and 'mark' or 'spot', essentially meaning 'non-point like', or failure to focus a point to a point [5]. It arises because of the off-axis rotation of the schlieren mirrors which results in a difference in path length along the optical centerline and periphery of the schlieren mirrors. This difference in path length is accounted for as astigmatism severity (Δf) as shown in Figure 8. Irrespective of the arduous efforts it is almost impossible to eliminate astigmatism completely from any off-axis mirror systems including the z-type schlieren imaging system. There is a geometrical formula for finding astigmatism severity in a z-type schlieren imaging system [5].

$$\Delta f = f.\frac{\sin^2\theta}{\cos\theta} \tag{18}$$

where θ is the mirror tilt angle. For small mirror tilt angle, Equation 18 is simplified to:

$$\Delta f = \frac{d^2}{4f} \tag{19}$$

where d is the diameter of the mirror. Smaller the value of Δf for a mirror with a given focal length f and off-axis angle θ, lesser will be the astigmatism severity.

Since the mirror tilt angle for the schlieren setup is 7.5°, it is not plausible to use the small angle approximation formula of Equation 19. Instead, using the formula stated in Equation 18, the astigmatism severity is obtained to be:

$$\Delta f = 400 \text{ mm}.\frac{\sin^2 7.5}{\cos 7.5}$$

$$\Delta f = 6.874 \text{ mm}$$

Since the distance between the sagittal and tangential focus, represented here by Δf is smaller than the focal length of the mirror by a factor of about 60, astigmatism would not be much of a problem for the schlieren system.

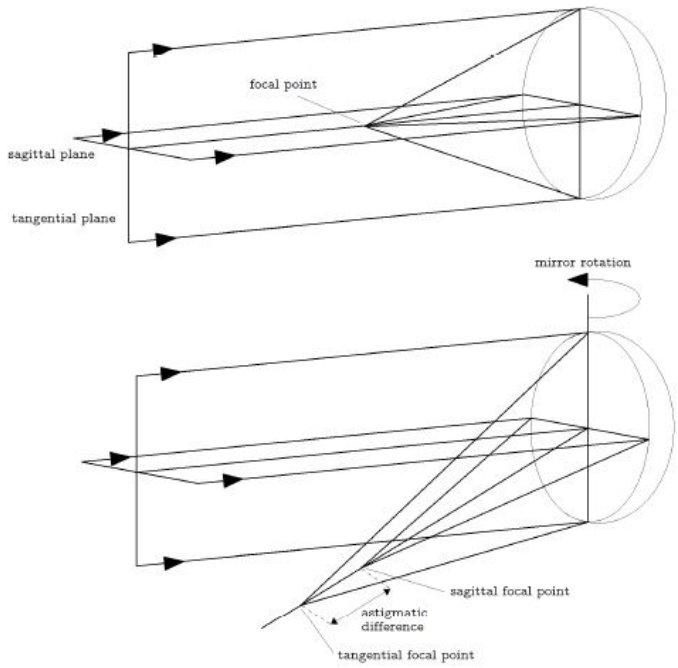

Figure 8: An illustration of astigmatism due to tilted mirror [6]

2.2 Equipment Setup Alignment

This section describes the overall configuration of the fabricated z-type 2-mirror schlieren setup, and the alignment of individual components that were used in the fabrication. Figure 9 shows the fabricated z-type 2-mirror schlieren setup. The main components of the setup are two mirror mounts allowing for the rotation of the mirror, two reflecting telescope parabolic mirrors, a light source stand with LED light, a knife-edge stand, a single reflex camera, and a wooden base.

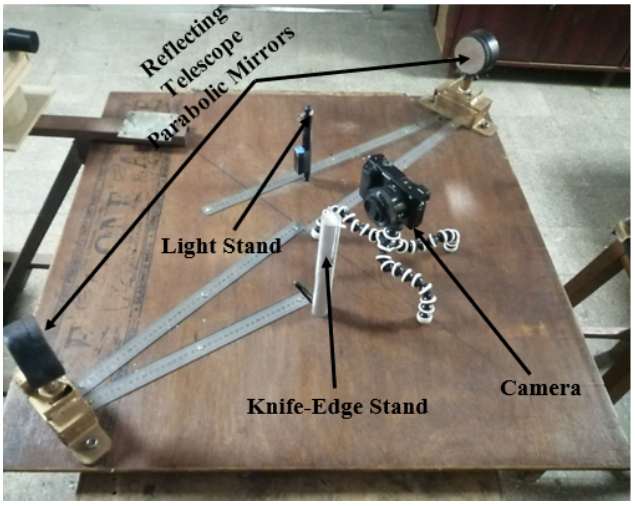

Figure 9: Fabricated z-type 2-mirror schlieren imaging system

For the purpose of achieving a clear image in the cutoff plane and on the camera, the schlieren system needs to be properly aligned. First of all, the reflecting telescope parabolic mirrors are placed on the opposite sides of the test section, maintaining a distance of 100 cm between each other. During the placement, the mirrors are aligned carefully maintaining a tilt angle of around 7.5°so that majority of the collimated light beam incident on the first mirror is reflected to the second mirror. These procedures are shown in Figure 10.

(a) (b)

Figure 10: (a) Adjustment of the illuminator, (b) Adjustment of the rotation and tilt controls of the schlieren mirror

The test section is maintained at the mid-distance of the two schlieren field mirrors. The light reflected from the first mirror traverses the test section before it reaches the second mirror. Careful alignment is needed to make sure that the test section is illuminated by the light collimated and reflected by the first mirror [6]. In this study, a 5-mm white LED light is chosen as the light source. It is kept in a light stand at a horizontal distance of 40 cm from the first mirror along the line inclined at 15°as shown in Figure 9. Using a piece of white A4 paper as screen, the tilt controls of the first mirror and second mirror is adjusted. The knife-edge is carefully placed at the focal point of the second mirror to cut-off certain portion of the source image. The knife-edge is adjusted multiple times to be sure if it is at the focal point of the second schlieren mirror. These procedures are shown in Figure 11.

(a) (b)

Figure 11: (a) Locating the focal point of second mirror, (b) Positioning the knife-edge to cut-off certain portion of the source image

The correction of the position of knife-edge was confirmed by placing a burning candle in the test section and observing its image in the camera with different amount of knife-edge cutoff. It is observed from Figure 12 that from the stand-point of the experimental works, cutoff of around 50% is ideal.

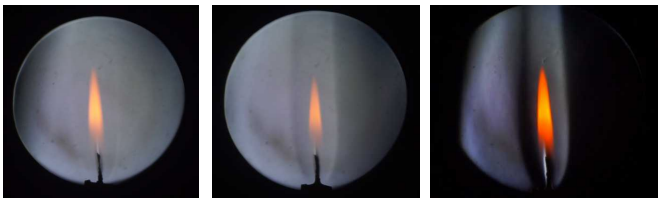

(a) (b) (c)

Figure 12: Schlieren photographs of thermal plume of a burning candle. The degree of knife-edge cutoff of the source image is (a) 0 %, (b) around 50 %, (c) almost 100 % cutoff. Placement of knife-edge:Vertical

3. Results and Discussion

3.1 Thermal plume of a Burning Candle

The schlieren setup was used to visualize the laminar convective plume of a burning candle. Since the mirror used in the schlieren setup is of diameter 7.6 cm giving a very limited field of view, the transition from laminar plume to turbulent plume is not captured. Despite this shortcoming, the laminar cylindrical flow of the candle is captured.An instability is created in the uniform laminar cylindrical flow of the candle plume by blowing into it. The transition in the flow is shown in Figure 13.

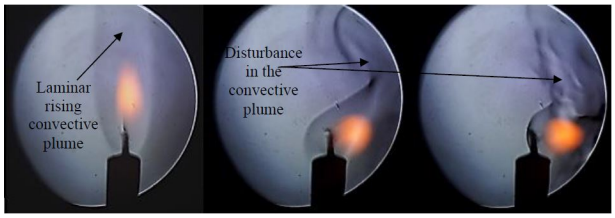

Figure 13: Uniform laminar cylindrical flow of a candle plume and its transition to disturbed flow captured in schlieren setup

3.2 Heated air near the periphery of soldering iron

The heat-transfer from the soldering iron onto the ambient air is captured in the schlieren setup. The hot air, having less density, naturally rises upwards. This phenomenon, captured by the schlieren setup is shown in Figure 14.

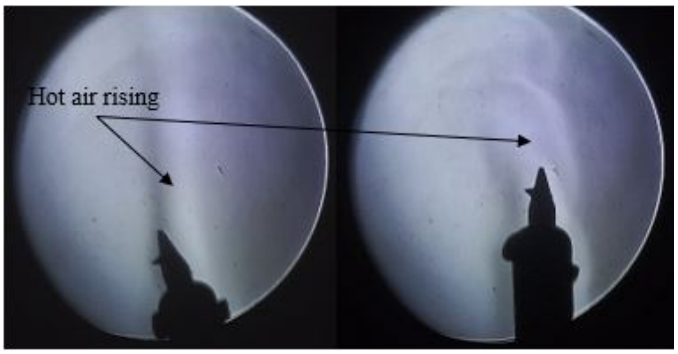

Figure 14: Rising hot air from the top of soldering iron

3.3 Flow through a Converging-Diverging (CD) Nozzle

A CD Nozzle, also called de Laval nozzle is a variable area passage which is used to accelerate gases to higher supersonic speeds. It consists of a converging section with minimum area occurring at a specific location called the throat. Downstream of the throat, the cross-sectional area starts to increase, thus creating the diverging section of the CD nozzle [7]. The nature of flow through the CD-nozzle for different pressure-ratios is observed with the fabricated z-type schlieren setup. For this study, a CD-nozzle is designed for exit Mach number of 1.4. For Mach 1.4, the parameters considered at the inlet chamber conditions and their resulting values in throat and exit conditions are shown in Table 1.

The contour for the diverging section of the nozzle is generated following the Method of Characteristics (MOC) incorporated in a MATLAB Code [8]. It is then followed with a CAD design and finally a realistic prototype of the nozzle is printed in a 3D printer. The material used for 3D printing is Acrylonitrile Butadiene Styrene (ABS). The experimental setup for the study of flow through the CD-nozzle are shown in Figures 15 and 16 respectively. The CAD geometry and the 3D printed prototype of the CD nozzle is shown in Figure 17. The detailed analysis of the design incorporating the reciprocating air-compressor, reservoir, polyurethane pipe and CD-nozzle could be found in [9]. The nature of flow through the CD-nozzle for Nozzle Pressure Ratio (NPR) ranging from 3.182 to 7 as observed in the z-type schlieren setup are shown in Figure 18.

Table 1: Values of parameters at different sections of the CD-nozzle

Parameters	Inlet chamber conditions	Throat conditions	Exit conditions
Pressure (Pascal)	322443.73	170341.15	101325.00
Temperature (Kelvin)	300	250	215.517
Density (kg/m^3)	3.74	2.37	0.86
Local velocity of sound (m/s)	...	316.938	294.269
Velocity of flow (m/s)	...	443.713	411.976

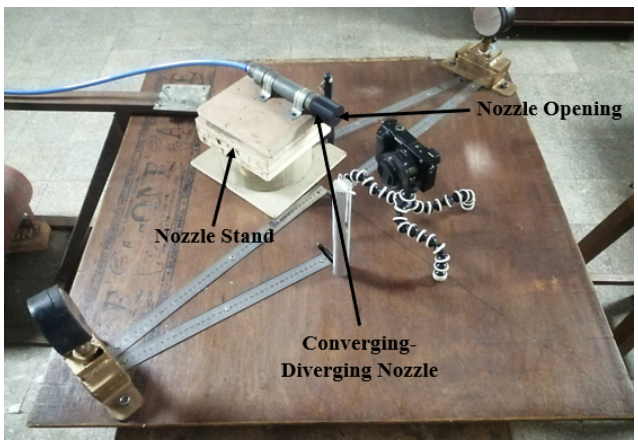

Figure 15: Experimental setup for visualizing flow through CD-nozzle at different NPR

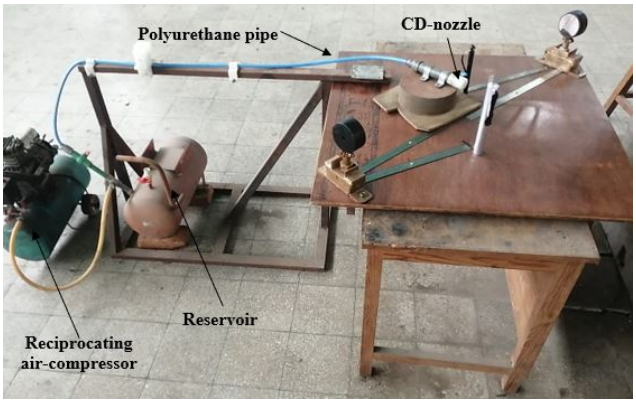

Figure 16: Experimental setup including the compressor section

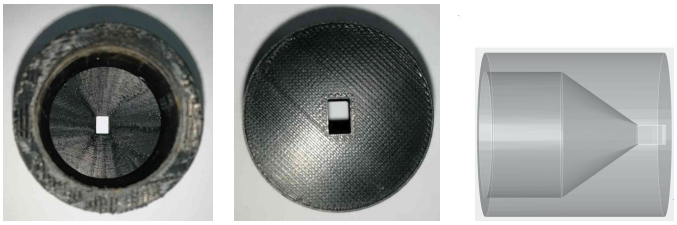

Figure 17: (a) Converging section of the CD-nozzle as observed in the 3D-printed prototype (b) Outlet section of the CD-nozzle as observed in the 3D-printed prototype (c) CAD Model of the CD-nozzle

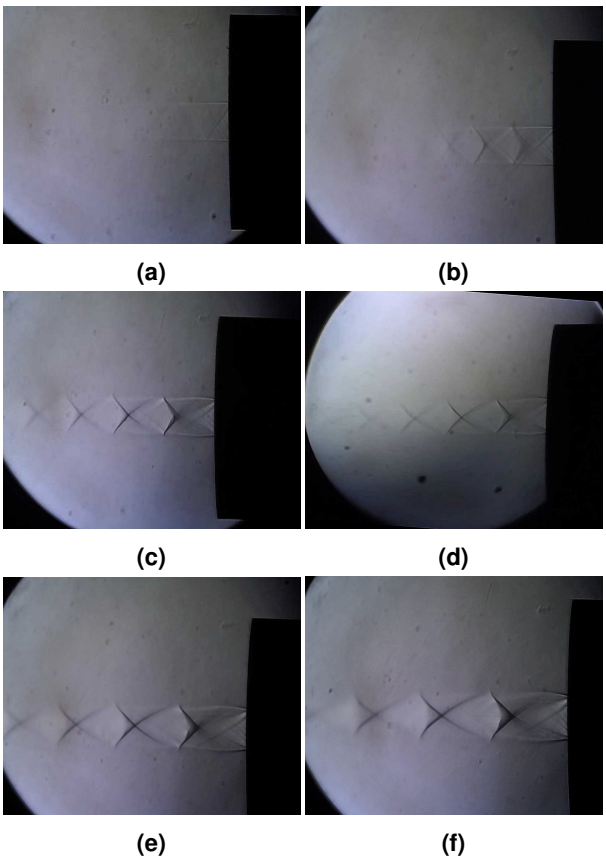

Figure 18: Flow through the CD-nozzle captured by z-type schlieren imaging setup at Nozzle-Pressure-Ratio of (a) 3.182 (isentropic condition), (b) 4, (c) 5, (d) 6, (e) 6.5, (f) 7

Supersonic flow through a CD-nozzle is characterised by the presence of shock structures. These shock structures also called 'shock diamonds', and they are formed when the nozzle pressure ratio (NPR) is off-design. When the actual NPR is less than the design value, the jet is said to be over-expanded and, when it is greater than the design NPR, it is said to be under-expanded [10]. The CD-nozzle designed for this study undergoes isentropic supersonic flow (perfectly expanded) for NPR of 3.182. The schlieren image of the flow at NPR 3.182 has some shock structures in it, meaning that the flow is not perfectly expanded. This implies losses via pressure drops in regions of pipe-bends in the setup itself.

Upon increasing the NPR, the shock diamond pattern (X-shaped structures) become distinct. These are formed when the nozzle exit pressure is higher than the atmospheric pressure. The flow thus becomes under-expanded and a series of expansion and compression waves are formed. The flow is called under-expanded because the nozzle cannot expand the gas/air enough resulting in the exit pressure being higher than the atmosphere pressure upon which the flow exhausts into. The nozzle by means of expansion fans decrease the pressure. The process through expansion fans is isentropic in nature. In this flow condition, a series of expansion waves and oblique shock waves are formed as shown in Figure 19 so that the nozzle could fulfill its objective of equalizing the exit pressure to the atmospheric pressure onto which the flow exhausts into.

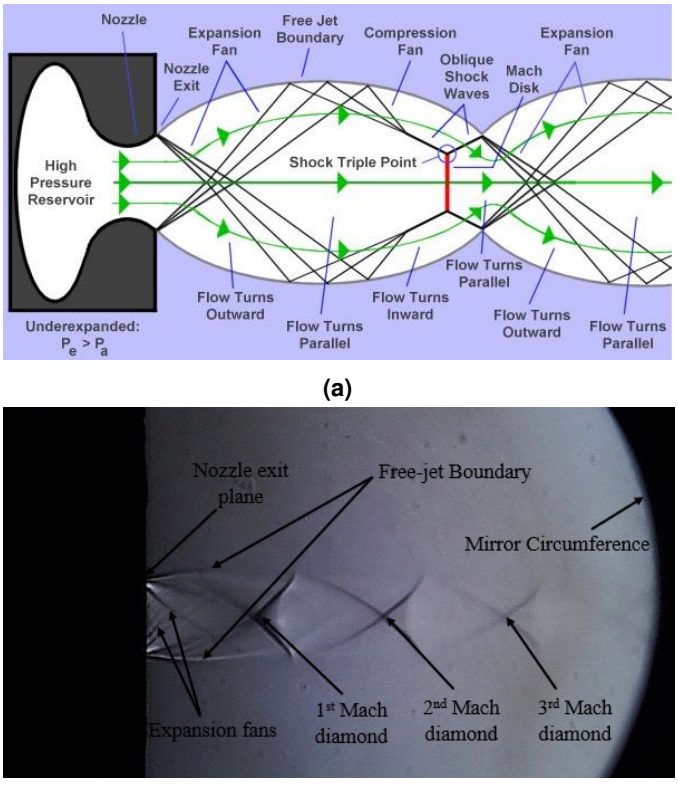

Figure 19: (a) Shock diamond pattern in an under-expanded flow [11], (b) Shock-diamond structures in an under-expanded flow through a CD-nozzle (NPR 7)

4. Conclusion

The fabricated z-type schlieren imaging system have the capacity to capture monochrome photographs of the schlieren object in the test section. This system is sensitive enough for qualitative analysis of simple subsonic phenomena such as thermal plume of a burning candle, heated air near the periphery of a soldering iron, as well as flow patterns of under-expanded jet through a CD-nozzle.

Acknowledgments

The authors are grateful to the Incubation, Innovation and Entrepreneurship Center (IIEC) of Institute of Engineering, Pulchowk Campus for providing the necessary devices and space for the fabrication of z-type schlieren setup and performing experimental study of different fluid-flow phenomena. Similarly, the authors are thankful towards Er. Mukesh Batajoo and Mr. Raman Bidari for their unwavering support during the fabrication of the z-type schlieren setup.

References

[1] W. Merzkirch. Visualization of flow. Available at https://www.thermopedia.com/content/1245/ (2011/02/11).

[2] Jean-Pierre Prenel and Dario Ambrosini. Flow visualization and beyond, 2012.

[3] Hubert Schardin. *The Toepler Schlieren Technique-Principles for its Application and Quantitative Analysis*. Phd thesis, 1934.

[4] E Mach and P Salcher. Photographische fixierung der durch projektile in der luft eingeleiteten vorgänge sitzungsberichte der kaiserlichen akademie der wissenschaften, 1887.

[5] Gary S Settles. *Schlieren and shadowgraph techniques: visualizing phenomena in transparent media*. Springer Science & Business Media, 2001.

[6] J.K. Nordberg. An assessment of colour schlieren photography for supersonic flows. Master's thesis, Luleå University of Technology, 2015.

[7] Karthik Remella and Marco Coderoni. Converging-diverging nozzle. Available at https://courses.ansys.com/index.php/courses/internal-compressible-flows/lessons/converging-diverging-nozzle-lesson-4/ (2023/08/03).

[8] Josh. Rocket-nozzle-design. Available at https://github.com/jte0419/Rocket_Nozzle_Design (2023/08/15).

[9] Bibek Gautam, Kamal Budhathoki, and Manjil Sitoula. Supersonic nozzle test using high pressure compressor. Bachelor's thesis, Institute of Engineering, Pulchowk Campus, Tribhuvan University, 2023.

[10] Priyadharshini Murugesan, Arjun Biju Kumar, Akhil Teja Kambhampati, Shashank Pillai, Girish Chandar Chandrasekar, Srikrishnan Ambattu Raghavannambiar, and Ratna Kishore Velamati. Numerical study of characteristics of underexpanded supersonic jet. *Journal of Aerospace Technology and Management*, 12, 2020.

[11] Jeff Scott. Shock diamonds and mach disks. Available at https://aerospaceweb.org/question/propulsion/q0224.shtml (2005/04/17).